

Cannabinoid- and lysophosphatidylinositol-sensitive receptor GPR55 boosts neurotransmitter release at central synapses

Sergiy Sylantsev^{a,1}, Thomas P. Jensen^{a,1}, Ruth A. Ross^{b,2}, and Dmitri A. Rusakov^{a,3}

^aDepartment of Clinical and Experimental Epilepsy, University College London Institute of Neurology, University College London, London WC1N 3BG, United Kingdom; and ^bInstitute of Medical Sciences, University of Aberdeen, Aberdeen AB25 2ZD, United Kingdom

Edited by Leslie Lars Iversen, University of Oxford, Oxford, United Kingdom, and approved February 12, 2013 (received for review July 3, 2012)

G protein-coupled receptor (GPR) 55 is sensitive to certain cannabinoids, it is expressed in the brain and, in cell cultures, it triggers mobilization of intracellular Ca²⁺. However, the adaptive neurobiological significance of GPR55 remains unknown. Here, we use acute hippocampal slices and combine two-photon excitation Ca²⁺ imaging in presynaptic axonal boutons with optical quantal analysis in postsynaptic dendritic spines to find that GPR55 activation transiently increases release probability at individual CA3-CA1 synapses. The underlying mechanism involves Ca²⁺ release from presynaptic Ca²⁺ stores, whereas postsynaptic stores (activated by spot-uncaging of inositol 1,4,5-trisphosphate) remain unaffected by GPR55 agonists. These effects are abolished by genetic deletion of GPR55 or by the GPR55 antagonist cannabidiol, a constituent of *Cannabis sativa*. GPR55 shows colocalization with synaptic vesicle protein vesicular glutamate transporter 1 in stratum radiatum. Short-term potentiation of CA3-CA1 transmission after a short train of stimuli reveals a presynaptic, Ca²⁺ store-dependent component sensitive to cannabidiol. The underlying cascade involves synthesis of phospholipids, likely in the presynaptic cell, but not the endocannabinoids 2-arachidonoylglycerol or anandamide. Our results thus unveil a signaling role for GPR55 in synaptic circuits of the brain.

Endocannabinoids play a major regulatory role in the functioning of neural circuitry. Classically, they are discharged by postsynaptic cells and target presynaptic cannabinoid type 1 (CB₁) receptors inhibiting neurotransmitter release (1, 2). Another documented cannabinoid target, the CB₂ receptor, is expressed almost entirely outside the brain, and little is known about any other cannabinoid signaling pathways. The cannabinoid-sensitive receptor G protein-coupled receptor 55 (GPR55) was identified and cloned a decade ago (3): Its presence in the brain, including the hippocampus, has been shown using quantitative PCR (4, 5). Although GPR55 activity can be modulated by certain phyto- and endocannabinoids (4, 6), recent studies have suggested that L- α -lysophosphatidylinositol (LPI), which activates GPR55 but not CB₁ or CB₂ receptors, could be its endogenous ligand (7, 8). Conversely, cannabidiol (CBD), a major constituent of *Cannabis sativa*, is a GPR55 antagonist, with low affinity for CB₁ receptors (4, 9). In cell cultures, activation of GPR55 evokes intracellular Ca²⁺ oscillations through an inositol 1,4,5-trisphosphate (IP₃)-sensitive mechanism mobilizing Ca²⁺ stores (8, 10, 11) whereas CBD can modulate neuronal Ca²⁺ depending on cell excitability (12). However, the GPR55 pharmacology is enigmatic, and its adaptive role in the brain remains unknown.

In the hippocampus, presynaptic Ca²⁺ stores contribute to repetitive release of glutamate (13, 14). Because GPR55 action has been attributed to Ca²⁺ stores, we asked whether these receptors influence transmission at CA3-CA1 synapses. To probe this mechanism at the single-synapse level, we combine electrophysiology with Ca²⁺ imaging in individual postsynaptic dendritic spines (“optical quantal analysis”) and in presynaptic axons traced from CA3 pyramidal cells into area CA1. We find that activation of GPR55 transiently increases release probability by elevating presynaptic Ca²⁺ through the activation of local Ca²⁺ stores. We also obtain evidence suggesting presynaptic expression of GPR55 and

its adaptive role in Ca²⁺-store-dependent short-term potentiation of CA3-CA1 transmission. Finally, our data point to LPI as a candidate endogenous ligand possibly released from presynaptic axons. By revealing the adaptive neurophysiological role of GPR55, these results also suggest a relevant neuronal target for CBD.

Results

Activation of GPR55 Transiently Increases the Frequency of Miniature Excitatory Postsynaptic Currents. Bath application of the GPR55 agonist LPI (4 μ M here and throughout) in acute hippocampal slices induced a prominent, 5- to 10-min boost in the frequency of miniature excitatory postsynaptic currents (mEPSCs) recorded in CA1 pyramidal cells (in 1 μ M tetrodotoxin; average increase over a 5-min interval after application $99 \pm 25\%$, mean \pm SEM here and thereafter; $P < 0.006$, $n = 8$), with no effect on the mEPSC waveform (Fig. 1A). The increase remained robust after 1 h of preincubation with the CB₁ receptor antagonist AM281 at 500 nM ($68 \pm 10\%$, $P < 0.003$, $n = 5$; Fig. 1E; this AM281 application protocol blocks the agonist action of WIN55,212-2; Fig. S1 A and B). In contrast, the facilitatory effect of LPI was abolished by the GPR55 antagonist CBD (1 μ M; change $7 \pm 4\%$, $n = 5$; Fig. 1B). Because spontaneous release at CA3-CA1 synapses partly depends on presynaptic Ca²⁺ stores (13), we asked whether Ca²⁺ store depletion interferes with the GPR55 action. The effect of LPI was abolished when Ca²⁺ stores were depleted with 10 μ M thapsigargin ($n = 6$) or 100 μ M ryanodine ($n = 6$; Fig. 1E). In contrast, suppressing glial metabolism with fluoroacetate (FAC, 1-h incubation at 5 mM; ref. 15) did not abolish the LPI-induced frequency increase ($47 \pm 11\%$, $n = 5$, $P < 0.001$; Fig. 1E). The GPR55 agonist O-1602 (100 nM here and throughout), a structural analog of CBD with low affinity for the CB₁ or CB₂ receptors (4), also increased the mEPSC frequency (by $118 \pm 33\%$, $n = 6$, $P < 0.017$; Fig. 1C, tests in wild-type C57BL mice). Importantly, the effects of either agonist were absent in the mice lacking the GPR55 gene (Fig. 1D and E). In contrast, Δ^9 -tetrahydrocannabinol (Δ^9 -THC) induced a small increase of the mEPSC frequency in slices from both CB₁ knockout (KO) and GPR55 KO mice (Fig. 1E), suggesting that Δ^9 -THC may have residual effects on multiple receptors. The undetectable effects of GPR55 agonists in KO animals were not due to the differences in average

Author contributions: S.S., T.P.J., R.A.R., and D.A.R. designed research; S.S. performed electrophysiological research; T.P.J. performed imaging, electrophysiology and immunocytochemical research; R.A.R. contributed new reagents/analytic tools; S.S., T.P.J., and D.A.R. analyzed data; and D.A.R. wrote the paper.

The authors declare no conflict of interest.

This article is a PNAS Direct Submission.

Freely available online through the PNAS open access option.

¹S.S. and T.P.J. contributed equally to this work.

²Present address: Department of Pharmacology and Toxicology, Faculty of Medicine, University of Toronto, Toronto, ON, Canada M5S 1A8.

³To whom correspondence should be addressed. E-mail: d.rusakov@ucl.ac.uk.

This article contains supporting information online at www.pnas.org/lookup/suppl/doi:10.1073/pnas.1211204110/-DCSupplemental.

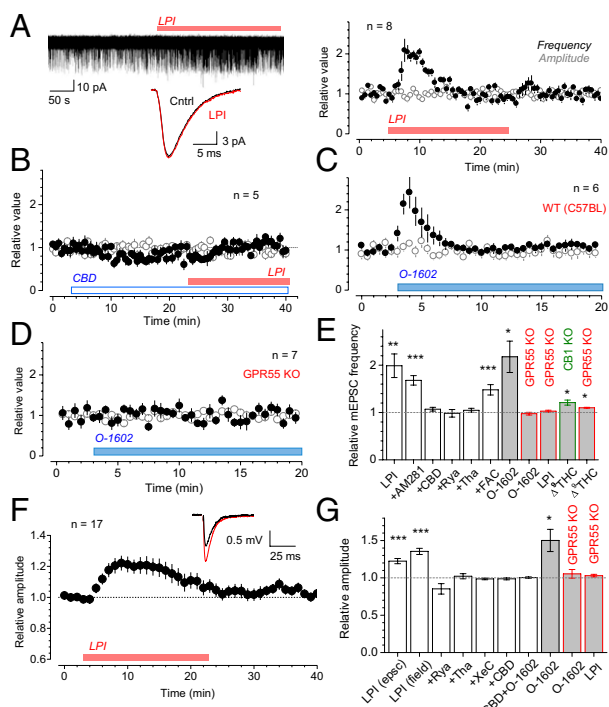


Fig. 1. Activation of GPR55 transiently boosts spontaneous and evoked CA3-CA1 transmission. (A) LPI (4 μM throughout) increases mEPSC frequency in CA1 pyramids (four traces superimposed), with no effect on the waveform (*Inset*). Plots are the average frequency (black) and amplitude (open) of mEPSCs during LPI application. Error bars (throughout): SEM. (B) GPR55 antagonist CBD (1 μM throughout) abolishes the effect of LPI. (C) GPR55 agonist O-1602 (100 nM throughout; C57BL mice) increases mEPSC frequency. (D) O-1602 has no effect on mEPSCs in GPR55 KO mice. (E) Relative changes in mEPSC frequency 3–5 min after application, as indicated: LPI ($n = 8$); LPI + AM281 (0.5 μM, 1-h incubation, $n = 5$), +CBD ($n = 5$), +ryanodine (+Rya, 100 μM throughout, $n = 6$), thapsigargin (+Tha, 10 μM throughout; $n = 6$), or +4 mM fluoroacetate (+FAC, 1-h incubation, $n = 5$); O-1602 in the wild-type mice ($n = 6$) and in GPR55 KO (change $-2 \pm 3\%$, $n = 7$); LPI in GPR55 KO (change $3 \pm 2\%$, $n = 7$), 4 μM Δ^9 THC (change $-2 \pm 3\%$, $n = 7$); LPI in GPR55 KO (change $3 \pm 2\%$, $n = 7$), 4 μM Δ^9 THC in CB₁ KO mice (Δ^9 THC, change $21 \pm 5\%$, $n = 5$), and in GPR55 KO mice ($10 \pm 1\%$, $n = 5$); white and gray columns: rats and mice, respectively, here and thereafter. * $P < 0.05$; ** $P < 0.01$; *** $P < 0.005$. (F) LPI transiently boosts evoked CA3-CA1 transmission (EPSCs and fEPSP data combined). (*Inset*) fEPSP example (black, baseline; red, averaged 3–5 min after application). Other notation as in A–D. (G) Relative changes in the evoked response 3–5 min after application, as indicated: LPI (EPSCs, $n = 21$, $P < 0.001$); LPI (fEPSPs, $n = 7$, $P < 0.001$); +Rya ($n = 6$), +Tha ($n = 6$), +10 μM (-)-Xestospingon C (+XeC, $n = 5$), and CBD (change $-1.1 \pm 1.5\%$, $n = 8$); O-1602 in CBD (CBD+O-1602; change $0.4 \pm 1.0\%$, $n = 5$), O-1602 in wild-type mice ($n = 4$, $P < 0.05$), and in GPR55 KO (change $5 \pm 6\%$, $n = 4$); and LPI in GPR55 KO (change $3 \pm 2\%$, $n = 9$).

mEPSC rates, which were similar among the species (Fig. S1C). Also, applying CBD at different time points after LPI did not change the time course of facilitation (Fig. S1D), suggesting that the latter is controlled downstream of GPR55 activation (e.g., by a lasting Ca^{2+} discharge from stores).

Activation of GPR55 Transiently Potentiates Evoked CA3-CA1 Responses. Both LPI and O-1602 transiently increased EPSCs or field excitatory postsynaptic potentials (fEPSPs) evoked in CA1 pyramids by stimulation of Schaffer collaterals. Again, Ca^{2+} store depletion with ryanodine, thapsigargin, or the IP₃ receptor blocker (-)-Xestospingon C (10 μM) abolished such increases, as did CBD (Fig. 1G). Reassuringly, the effects of either GPR55 agonist were absent in GPR55 KO mice (Fig. 1G), whereas the baseline probability of evoked release in these animals was similar to that in wild type (WT; Fig. S1E). Overall, GPR55 agonists had a somewhat greater effect on spontaneous compared

with evoked responses (Fig. 1E and G), possibly because mEPSCs depend on Ca^{2+} store discharges more directly than do evoked responses (13, 14).

Optical Quantal Analysis Establishes That GPR55 Activation Increases Release Probability. Potentiation of evoked responses by GPR55 agonists was paralleled by a decreased paired-pulse ratio (PPR, 50-ms interval), suggesting an increase in release probability, P_r (Fig. S2A). However, PPR is not always a reliable indicator of P_r because it might also reflect changes in recruitment of activated synapses (16). To gauge P_r more directly, we monitored Ca^{2+} in dendritic spines of CA1 pyramids (Fig. 2A) representing individual CA3-CA1 synapses. First, GPR55 agonists on their own had no effect on Ca^{2+} inside the spine over ~10 min of recording (Fig. 2B) although these spines contained functional Ca^{2+} stores: Two-photon spot uncaging of the Ca^{2+} store ligand IP₃ inside the spine head in a subset of experiments invariably evoked a Ca^{2+} rise characteristic of Ca^{2+} stores (17) ($\Delta G/R$: 0.407 ± 0.050 , $n = 4$, $P < 0.007$; Fig. 2B). Postsynaptic Ca^{2+} stores were therefore insensitive to GPR55 activation (Fig. 1E and G). Second, we used the optical quantal analysis (18, 19), which we adapted earlier (20), to monitor individual evoked release events at CA3-CA1

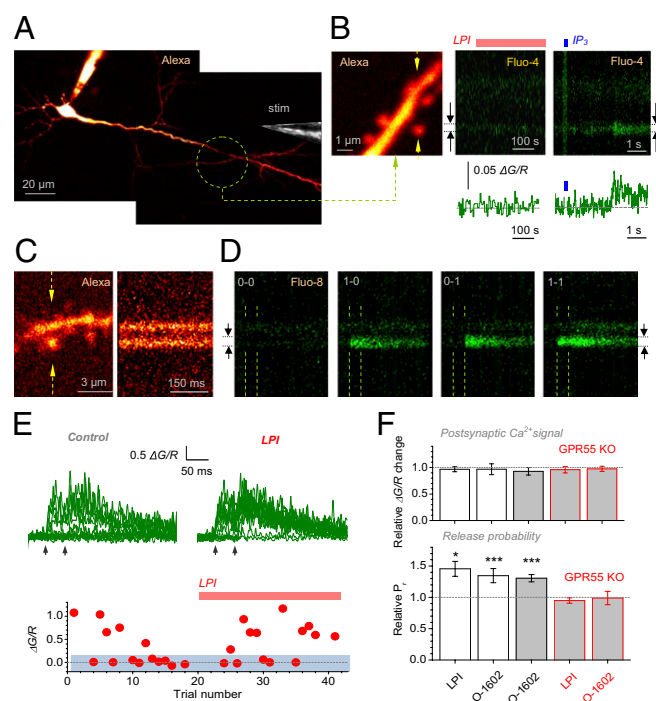


Fig. 2. Activation of GPR55 increases release probability at individual CA3-CA1 synapses. (A) Example of recorded CA1 pyramidal cell (Alexa channel); stimulating pipette shown [stim; differential interference contrast (DIC) channel, fragment]. (B *Left*) Dendritic fragment from the region indicated in A; arrows, linescan position. (*Center*) LPI (4 μM) induces no Ca^{2+} changes in the spine head (1 Hz linescan); one-cell example: arrows, linescan integration segment. (*Right*) Uncaging IP₃ (whole-cell, 400 μM; 10 5-ms pulses at 40 Hz, $\lambda_{u}^{2P} = 720$ nm, blue bar) inside the same spine induces a prominent Ca^{2+} signal (trace). (C) Dendritic fragment of interest (*Left*; arrows, linescan position) and linescan (*Right*; 500 Hz) in Alexa channel ("red" fluorescence). (D) Linescans of the fragment shown in B in Fluo-4 channel. Paired stimuli (dotted lines) induce four types of Ca^{2+} responses in one spine: 1 and 0, success and failure, respectively; other notation as in B. (E *Upper*) Ca^{2+} fluorescence time course (recorded as in D) before and after LPI application; Arrows, stimulus onsets. (E *Lower*) Amplitudes of first Ca^{2+} responses in the same experiment. Blue shade, the range of failure (twice the baseline noise SD). (F) Relative change in the Ca^{2+} $\Delta G/R$ amplitude (*Upper*) and P_r (*Lower*) in response to: LPI ($n = 5$) and O-1602 ($n = 4$) in rats, O-1602 in wild type ($n = 4$), and LPI and O-1602 in GPR55 KO mice ($n = 5$ and $n = 4$, respectively).

synapses (Fig. 2 *C* and *E*). By documenting successes and failures of evoked Ca^{2+} rises in a postsynaptic dendritic spine, this approach provides direct readout of single-synapse P_r . P_r was increased by both LPI (by $46 \pm 12\%$, $n = 5$, $P < 0.02$) and O-1602 (by $35 \pm 6\%$ in the rat, $n = 4$, $P < 0.009$; and by $31 \pm 6\%$ in WT mice, $n = 4$, $P < 0.002$) for 10–15 min after application, without affecting the Ca^{2+} signal amplitude (Fig. 2 *E* and *F* and Fig. S2*B*). Again, the effect of agonists was absent in the GPR55 KO mice (change $-5.1 \pm 4.3\%$, $n = 5$, and $-1.2 \pm 5.3\%$, $n = 4$, respectively; Fig. 2*F* and Fig. S2*C*).

GPR55 Receptors Engage Ca^{2+} Store Discharges in Individual Presynaptic Boutons. Elevations of presynaptic Ca^{2+} is a classical mechanism to control P_r . To monitor Ca^{2+} in axonal boutons forming CA3-CA1 synapses, we held CA3 pyramidal cells in whole-cell mode and, in a number of fortuitous cases, traced the cell axon into area CA1 (Fig. 3*A*), adapting identification criteria established by us previously (21). In all traced boutons, LPI induced a prominent oscillatory elevation of Ca^{2+} lasting 5–15 min with the average amplitude ($\Delta G/R$: 0.175 ± 0.048 , $n = 5$, $P < 0.03$) comparable to spike-evoked Ca^{2+} entry in such boutons ($\Delta G/R$: 0.118 ± 0.019 , $n = 7$, $P < 0.001$; Fig. 3*B* and *E*). O-1602 induced a similarly long-lasting Ca^{2+} response in all recorded boutons ($\Delta G/R$: 0.082 ± 0.012 , $n = 5$, $P < 0.003$; Fig. 3*E* and Fig. S3*A–C*). These elevations were abolished by ryanodine or thapsigargin, which rapidly discharged Ca^{2+} stores upon application ($n = 5$; Fig. 3*C* and *E* and Fig. S3*D* and *E*); at the same time, however, LPI had no detectable influence on Ca^{2+} homeostasis in CA1 astrocytes (Fig. S4). Similarly, 1 μM CBD suppressed the effects of both LPI and O-1602 (applied ~ 4 min after LPI; $\Delta G/R$ 0.000 ± 0.002 , $n = 4$ traced axons; Fig. 3*E*). In contrast to GPR55 agonists, the CB_1 receptor agonist WIN55,212-2 (500 nM) had no effect on presynaptic Ca^{2+} ($n = 7$; Fig. 3*E*) although it could robustly activate CB_1 receptors (Fig. S14). Again, in GPR55 KO mice, LPI and O-1602 applied consecutively (~ 4 -min interval) produced no elevation of presynaptic Ca^{2+} ($\Delta G/R$ 0.0016 ± 0.0011 , $n = 5$; Fig. 3*D*), whereas spike-evoked Ca^{2+} entry remained robust ($\Delta G/R$ 0.089 ± 0.013 , $n = 6$; $P < 0.001$; Fig. 3*D* and *E*). These observations thus suggested that the GPR55-induced increase in P_r (Fig. 2) involves discharges from presynaptic Ca^{2+} stores.

GPR55 Is Expressed in Stratum Radiatum Showing Colocalization with Synaptic Vesicles. To label GPR55 in acute slices we used an Alexa Fluor 488 conjugated CTFL antibody (C terminus binding; provided by Ken Mackie, Indiana University, Bloomington, IN; Fig. 4*A*). Aiming at unbiased evaluation, we quasirandomly sampled stratum radiatum and stratum pyramidale and applied an unsupervised (blind) image segmentation algorithm for puncta detection (Fig. 4*B* and *SI Methods*). WT samples showed profoundly enhanced puncta labeling compared with GPR55 KO in both hippocampal areas (Fig. 4*C*, magnified in Fig. S5*A*). The puncta density appeared lower than the occurrence of CA1-CA3 synapses ($\sim 2 \mu\text{m}^{-3}$), suggesting a relatively low success rate of epitope binding. To examine presynaptic location of GPR55, we tested whether it was colocalized with the glutamatergic synaptic vesicle protein vesicular glutamate transporter 1 (VGLUT1) (Fig. 4*D*). An image analysis algorithm that minimizes spurious colocalization due to bleed-through, residual or background fluorescence showed significant colocalization compared with scrambled images (Fig. 4*E* and *F* and *SI Methods*), thus associating GPR55 expression with individual Schaffer collateral boutons (Fig. S6). In addition, we tested GPR55 expression in presynaptic CA3 pyramids by using a recently developed fluorescent ligand, which has a selectively high affinity to GPR55, Tocrifluor T1117 (22). We applied this water-soluble ligand extracellularly by using a pressure pipette placed near the CA3 pyramid (Alexa Fluor 488 was cojected to monitor nonspecific uptake; Fig. S5*B*). Strikingly, cytosolic compartments of live CA3 pyramidal cells in slices from WT and CB_1 KO animals, but not GPR55 KO animals, readily accumulated Tocrifluor T1117 (Fig. S5*C*).

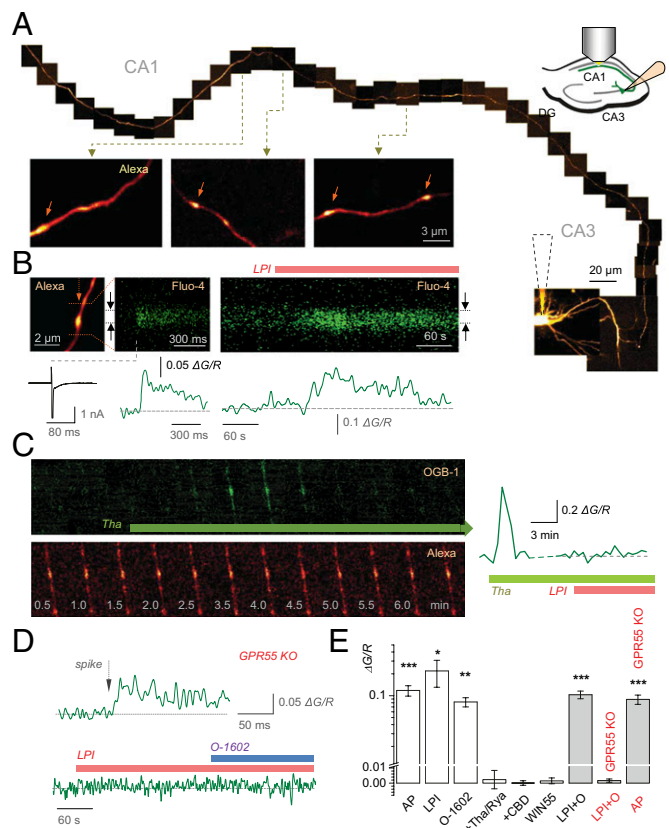


Fig. 3. GPR55 activation prompts presynaptic Ca^{2+} elevation at CA3-CA1 synapses. (A) Tracing a CA3 pyramidal cell axon into CA1 (10–15 μm Kalman-averaged stacks, collage). Bouton examples shown are magnified. (Inset) Experiment diagram. (B) An individual bouton [Upper Left; arrows, linescan position] showing rapid spike-evoked Ca^{2+} entry (traces; Upper Center, 500 Hz linescan) and a slow LPI-induced Ca^{2+} elevation (Upper Right; 1 Hz linescan; black arrows, linescan region of interest). (B Lower) $\Delta G/R$ (Methods) time course. (C) CA1 presynaptic bouton seen in green (Upper) and red (Lower) channels showing prominent Ca^{2+} rise induced by thapsigargin (Tha, frame time points shown) but no effect of the subsequent LPI application (Right; $\Delta G/R$ recording period extended). (D) In GPR55 KO, CA3-CA1 boutons show robust spike-induced Ca^{2+} entry (Upper) but no response to LPI and O-1602 (Lower); other notation as in B. (E) The average Ca^{2+} $\Delta G/R$ signal evoked by: one action potential (AP, $n = 7$), LPI ($n = 5$), O-1602 ($n = 5$), LPI + Tha or Rya ($n = 5$; average $\Delta G/R$: 0.002 ± 0.006 , combined data; difference with the LPI-induced $\Delta G/R$ at $P < 0.008$), LPI followed by O-1602 (in ~ 4 min) in CBD ($\Delta G/R = 0.0015 \pm 0.002$, $n = 4$), and the CB_1 receptor agonist WIN 55,212-2 (WIN55, $n = 7$; $\Delta G/R = 0.0015 \pm 0.0019$, $n = 7$, difference with the LPI-induced signal at $P < 0.005$), LPI followed by O-1602 in wild-type mice (LPI+O, $\Delta G/R$ 0.10 ± 0.01 , $n = 5$, $P < 0.0012$), and in GPR55 KO ($\Delta G/R$ 0.0016 ± 0.0011 , $n = 5$), one spike in GPR55 KO mice (AP in red, $\Delta G/R$ 0.089 ± 0.013 , $n = 6$, $P < 0.001$).

Short-Term Postburst Synaptic Potentiation Has a GPR55-Dependent Component. Although the above results relate GPR55 to enhanced glutamate release and presynaptic Ca^{2+} stores, they do not reveal whether this mechanism is engaged endogenously. Short bursts of synaptic discharges transiently potentiate CA3-CA1 transmission, which is thought to depend on presynaptic Ca^{2+} elevations (23). We asked whether this type of postburst potentiation (PBP) involves GPR55. We evoked PBP by applying 10 electric stimuli at 100 Hz to Schaffer collaterals, a protocol compatible with burst activity of CA3 pyramids in situ (longer-term potentiation was blocked with 50 μM (2R)-amino-5-phosphonovaleric acid, an NMDA receptor antagonist). To examine the role of GPR55, PBP was induced twice ~ 20 min apart, and CBD was added shortly after the first induction. We found that CBD inhibited PBP substantially (in rats by $52 \pm 15\%$, $n = 5$, $P < 0.018$; in WT mice by $63 \pm 16\%$, $n = 7$, $P < 0.009$), whereas in control slices, with no

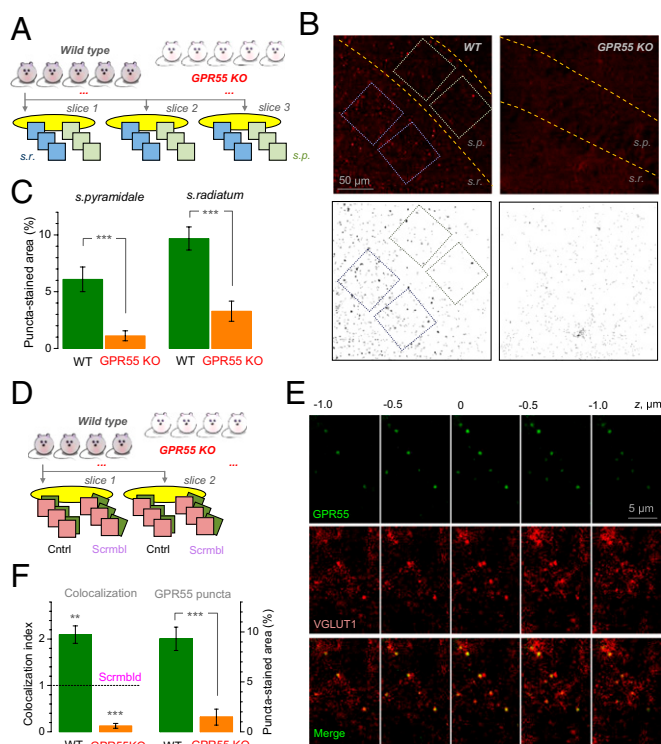


Fig. 4. Expression of GPR55 in area CA1 and its colocalization with synaptic vesicle protein VGLUT1. (A) Experimental design for GPR55 immunolabeling analyses: five WT and GPR55 KO mice samples; three slices in each animal; three and quasirandomly selected ROIs ($\sim 66 \times 66 \mu\text{m}$) in stratum radiatum and stratum pyramidale. Two-way ANOVA design is shown (gene deletion and stratum area being fixed factors). (B Upper) Example of area CA1 labeled for GPR55 in WT and GPR55 KO. Dotted rectangles, ROIs (higher resolution shown in Fig. S5A). (B Lower) Outcome of blind image segmentation separating the puncta in the images above (Methods). (C) Relative area of puncta in WT and KO. $***P < 0.001$ (t test, $n = 5$ and $n = 5$) [ANOVA results: GPR55 gene-specific puncta, $P < 0.001$ ($F = 52.0$); effect of region, $P < 0.02$ ($F = 8.53$); "hippocampal region-gene deletion" interaction, $P > 0.38$ ($F = 0.82$)]. (D) Experimental design for GPR55-VGLUT1 colocalization analyses: four WT and four GPR55 KO mice; two slices in each stained for GPR55 and VGLUT1; and three ROIs per slice. Diagram depicts pairs of original and "scrambled" ROIs analyzed to obtain an unbiased colocalization indicator (SI Methods). (E) An example stratum radiatum fragment labeled with GPR55 and VGLUT1 antibodies, seen in several serial confocal sections $0.5 \mu\text{m}$ apart, as indicated. (F Left) Colocalization index for WT and GPR55 KO samples (pixels from GPR55 and VGLUT1 channels that meet colocalization criteria minimizing bleed-through, background or residual fluorescence; numbers relative to those in scrambled images from WT, Scrambl; SI Methods); $**P = 0.01$ (three-way ANOVA nested, $F = 34.1$; Methods); $***P < 0.003$. (Right) Relative area of puncta in WT and KO, as in C, in this sample, $***P < 0.005$ (independent-sample t test).

CBD application, PBP could be induced twice to the same level, without rundown or enhancement (Fig. 5A and Fig. S7A and B). CBD was similarly active at $0.2 \mu\text{M}$ but, critically, it had no effect on PBP in the GPR55 KO mice (Fig. 5B and C, red arrow); furthermore, baseline PBP in GPR55 KO was one-third of that in the WT ($11 \pm 2\%$ and $31 \pm 6\%$; $n = 7$ and $n = 6$, respectively; difference at $P < 0.007$). Again, PBP induction was not affected by the CB_1 receptors antagonist AM281 (500 nM ; Fig. 5C), and loading the postsynaptic cell with a Ca^{2+} chelating solution [100 mM Cs-1,2-bis(o-aminophenoxy)ethane- N,N,N',N' -tetraacetic acid (BAPTA), whole-cell; Methods] had no effect on the CBD-sensitive PBP component (Fig. 5C and Fig. S7C).

GPR55-Dependent Potentiation Requires Synthesis of Phospholipids but Not Endocannabinoids. We next attempted to identify the candidate endogenous ligand of GPR55, starting with the

endocannabinoids anandamide and 2-arachidonoylglycerol (2-AG). We incubated slices with 100 nM JNJ 1661010 or with either 20 nM or $1 \mu\text{M}$ URB-597 (inhibitors of fatty acid amide hydrolase) for 1 h to prevent anandamide hydrolysis. This application had no effect on the CBD sensitivity of PBP (Fig. 5C and Fig. S7D–F). We also blocked monoacylglycerol lipase, the enzyme involved in hydrolysis of 2-AG, using *N*-arachidonyl maleimide (NAM, $1 \mu\text{M}$ or $10 \mu\text{M}$; 1 h), and blocked the production of 2-AG with the diacylglycerol lipase inhibitor, RHC 80267 (RHC, $10 \mu\text{M}$) for 1 h. Again, this had no detectable effect on the CBD-sensitive PBP (Fig. 5C and Fig. S7G–I). Because LPI has been suggested as an endogenous GPR55 agonist, we attempted to suppress metabolic pathways that control synthesis of phospholipids, by incubating slices for 1 h with YM 26734 ($20 \mu\text{M}$) and arachidonyl trifluoromethyl ketone (AACOCF3) ($10 \mu\text{M}$), which

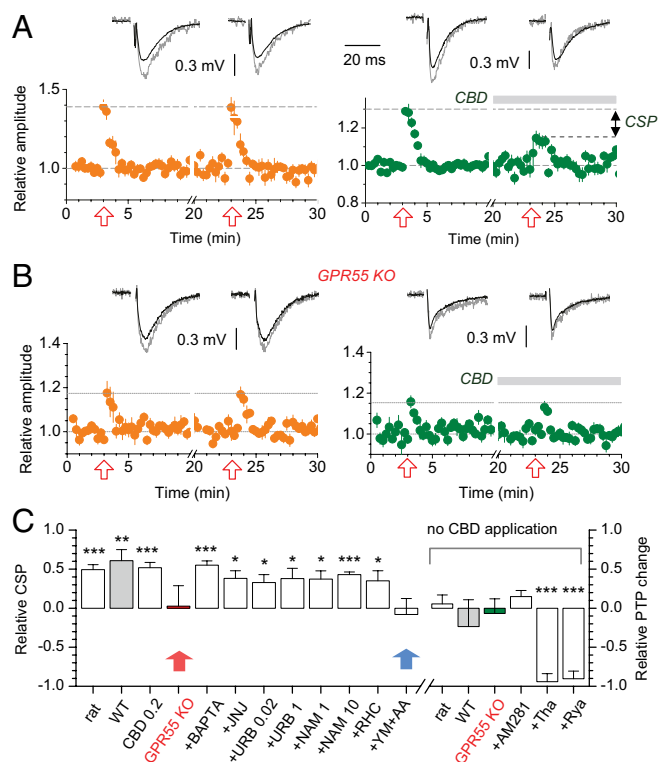


Fig. 5. PBP at CA3-CA1 synapses has a GPR55-dependent component. (A Lower) Time course of PBP (fEPSP amplitude/slope monitored) induced twice by 10 pulses at 100 Hz (arrows) in control (Left; $n = 5$) and test (Right; $n = 5$; CBD application shown) groups of rats. (A Upper) Examples of baseline (black), 10 fEPSPs averaged and potentiated (gray, first fEPSP posttrain) responses; CSP, CBD-sensitive PBP. (B) As in A but in GPR55 KO mice. (C) Results of experiments similar to A and B, in different test conditions. Shown in the left ordinate are the following: relative CSP in rats ($n = 7$; $***P < 0.001$), WT C57 mice (WT, $n = 6$; $**P < 0.0075$), GPR55 KO ($n = 7$), with CBD applied at $0.2 \mu\text{M}$ ($n = 5$; $***P < 0.003$); with 100 mM Cs-BAPTA in whole-cell pipette (+BAPTA, EPSC amplitudes, $n = 5$; $***P < 0.001$), and after 1-h incubation with fatty acid amide hydrolase inhibitors JNJ 1661010 (100 nM ; +JNJ, $n = 5$; $*P < 0.017$), URB-597 (0.02 and $1 \mu\text{M}$; +URB 0.02 and +URB 1, respectively, $n = 5$, $*P < 0.04$), monoacylglycerol lipase inhibitor *N*-arachidonyl maleimide (1 and $10 \mu\text{M}$; +NAM 1 and +NAM 10, respectively, $n = 5$; $*P < 0.05$, $***P < 0.005$), diacylglycerol lipase inhibitor RHC 80267 ($10 \mu\text{M}$, +RHC, $n = 5$, $*P < 0.038$), and phospholipase A_2 inhibitors YM 26734 and AACOCF3 applied together (20 and $10 \mu\text{M}$, respectively; +YM+AA, $n = 5$, $P = 0.71$; red arrow). Shown in the right ordinate are the following: relative difference between the first and second PBP controls in rats ($n = 10$, $P > 0.53$), WT C57 mice (WT, $n = 5$, $P > 0.33$), and GPR55 KO mice (GPR55 KO, $n = 5$, $P = 0.74$); also showing PBP sensitivity to 500 nM AM281 (+AM281, $n = 5$, $P > 0.13$), $10 \mu\text{M}$ thapsigargin (+Tha, $n = 5$, $***P < 0.001$), and $100 \mu\text{M}$ ryanodine (+Rya, $n = 5$, $***P < 0.001$) added after the first PBP induction.

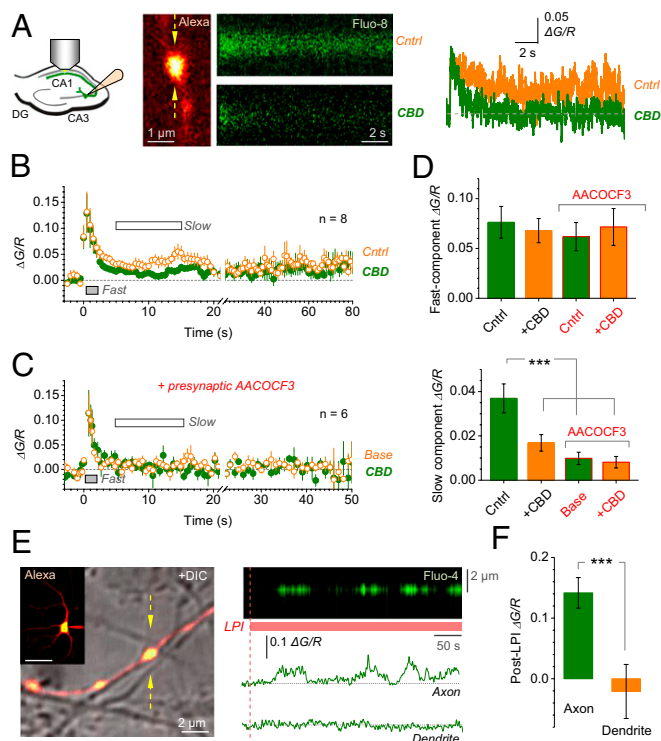


Fig. 6. Presynaptic Ca^{2+} rise is inhibited by CBD or by presynaptic suppression of PLA_2 and can be induced in cultured cell axons with no glia in the neighborhood. (A *Left*) Experiment diagram. (A *Center*) In example bouton (Left, as in Fig. 3A), and its Ca^{2+} response to 10 spikes at 100 Hz (500 Hz line scan, Fluo-8 channel) before (Upper) and 10 min after CBD application (Lower). (A *Right*) Ca^{2+} responses expressed as $\Delta G/R$. (B) Average Ca^{2+} response to the 10-spike burst (onset $t = 0$) monitored in CA3-CA1 presynaptic boutons for 80 s ($n = 8$) before (orange) and ~ 20 min after (green) CBD application. Averaging periods for the fast (0–2 s after burst) and slow (5–15 s) Ca^{2+} elevations are shown. (C) Experiments as in B but with the phospholipid synthesis inhibitor AACOCF3 (10 μM) in the cell ($n = 6$). (D) Effect of CBD on fast (Upper) and slow (Lower) Ca^{2+} signals; $***P < 0.001$. (E *Left*) A cultured hippocampal neuron held in whole-cell (Inset, Alexa channel) with traced axonal presynaptic boutons (merged with DIC image; postsynaptic dendrite can be seen); arrows, linescan position. (Scale bar: 50 μm .) (E *Right*) (Upper) Ca^{2+} signal in the bouton shown on the left, during bath application of 4 μM LPI, as indicated. (Lower) Same Ca^{2+} response expressed as $\Delta G/R$ (Upper) and in the dendrite from the same cell (Lower). (F) Effect of LPI on Ca^{2+} in axonal boutons ($n = 6$; for comparison, typical spike-induced $\Delta G/R$ amplitude in these axons were 0.13–0.15) and dendrites ($n = 4$) of recorded cells as in E; $***P < 0.001$.

inhibit phospholipase A_2 (PLA_2). Strikingly, this treatment did abolish the CBD-sensitive PBP component (Fig. 5C, blue arrow; and Fig. S7J). Finally, short-term PBP was completely blocked by 10 μM thapsigargin or by 100 μM ryanodine (Fig. 5C and Fig. S8), thus confirming the reliance of PBP on Ca^{2+} stores.

Short Spike Bursts Induce Slow Axonal Ca^{2+} Elevations Sensitive to GPR55 and to Presynaptic Blockade of LPI Synthesis. To test whether the CBD-sensitive PBP involves presynaptic Ca^{2+} changes, we monitored Ca^{2+} signals evoked in axonal boutons of CA3 pyramidal cells (as in Fig. 3A) by 10 spikes at 100 Hz, before and after application of CBD. In baseline conditions, the spike burst induced not only a rapid Ca^{2+} increment reflecting spike-evoked Ca^{2+} entry, but also a long (>80–90 s) oscillatory Ca^{2+} elevation (Fig. 6A and B; Ca^{2+} monitoring beyond 1–2 min was unreliable because of issues pertinent to focus fluctuations, photobleaching, and phototoxicity). Application of CBD inhibited the slow Ca^{2+} signal component (by $57 \pm 7\%$ over 5–15 s after burst, $P < 0.001$, $n = 8$), without affecting the initial rapid Ca^{2+}

entry (Fig. 6B), thus implicating GPR55 into the PBP-dependent presynaptic Ca^{2+} elevation. Strikingly, when we loaded the selective PLA_2 inhibitor AACOCF3 (10 μM) into the recorded cell, the slow (but not fast) component of postburst Ca^{2+} elevation was suppressed (from $\Delta G/R$ 0.037 ± 0.006 in control to 0.010 ± 0.003 with AACOCF3, $P < 0.001$, $n = 8$ and $n = 6$, respectively) and it was insensitive to CBD (Fig. 6C and D). Because in these tests any significant transmembrane escape of somatically loaded AACOCF3 would prevent it from reaching the remote axonal bouton at any effective level, this result associates the CBD-sensitive presynaptic Ca^{2+} elevation with axonal release of a candidate ligand (possibly LPI or a derivative).

LPI Induces Ca^{2+} Rises in Cultured Cell Axons Exposed to Bath Medium. Although the findings above point to the role of presynaptic GPR55, they do not rule out the involvement of GPR55 expressed in astroglia, which closely approach CA3-CA1 synapses (24). To address this issue more directly, we monitored Ca^{2+} in the axonal boutons of cultured hippocampal cells that are exposed to the bath medium, with no glia present in the surrounding environment (Fig. 6E, *Left* and *Methods*). Application of LPI-induced robust oscillatory Ca^{2+} rises in such boutons, but not in dendritic compartments of recorded cells (Fig. 6E, *Right*, and F). This result argues against the contribution of glia to GPR55-dependent presynaptic Ca^{2+} elevations documented here (although this finding does not exclude the expression and physiological roles of astroglial GPR55 per se).

Discussion

Our results have unveiled an adaptive role for the enigmatic cannabinoid-sensitive receptor GPR55 in the brain. Two structurally dissimilar agonists (LPI and O-1602), which have different target receptor pools overlapping at GPR55, prompted transient increases in P_r at CA3-CA1 synapses, the phenomenon confirmed by using an “optical quantal analysis” of Ca^{2+} responses in postsynaptic dendritic spines. The underlying mechanism involves Ca^{2+} -store dependent presynaptic Ca^{2+} elevations recorded in axonal boutons traced from CA3 pyramids into area CA1. Combination of pre- and postsynaptic Ca^{2+} imaging has thus provided direct evidence for GPR55 function at the single-synapse level, with the receptor identity validated by using GPR55 KO animals. Interestingly, although the GPR55-dependent presynaptic Ca^{2+} rise was comparable with the spike-evoked signal, it did not trigger neurotransmitter release. This result suggests that the GPR55-activated Ca^{2+} source was further away from the release machinery than spike-activated Ca^{2+} channels. We have also obtained evidence for GPR55 expression in stratum radiatum, also suggesting its submicron proximity to glutamatergic synaptic vesicles expressing VGLUT1.

Previous work associated GPR55 actions with $\text{G}\alpha_{12/13}$ G protein and RhoA-mediated, IP_3 -dependent Ca^{2+} stores (8, 10, 11). However, we have detected the role of both IP_3 and non- IP_3 stores. Indeed, various Ca^{2+} stores are thought to interact within small axonal boutons, and further studies are needed to understand the interplay involved. Importantly, GPR55 could be activated by physiologically relevant bursts of synaptic discharges, thus contributing to short-term PBP of transmission. Again, this involvement depends on presynaptic Ca^{2+} stores, consistent with their role in use-dependent release enhancement (14, 17). Our data report the transient nature of GPR55-induced facilitation: This phenomenon might reflect the finite capacity, or a relatively slow recharge rate, of Ca^{2+} stores triggered by GPR55 activation. Another possible explanation is internalization of activated GPR55, which is possibly reflected in cellular uptake of T1117 detected here.

GPR55 agonists did not activate functional postsynaptic Ca^{2+} stores, and postsynaptic Ca^{2+} chelation had no effect on the GPR55-dependent PBP. These results argue against the postsynaptic retrograde signaling involved in the observed P_r changes. Similarly, GPR55 actions were insensitive to glial poisoning, and GPR55 agonists had no effect on astrocytic Ca^{2+} . Furthermore, in

hippocampal cultures, LPI evoked Ca^{2+} rises in axons exposed to bath medium, with no glia present nearby. These data suggest little role of astroglia in the observed phenomena (although they do not rule out yet-unknown functions of glial GPR55, if such are present). GPR55-dependent PBP remained intact when we interfered with the metabolism of classical endocannabinoids 2-AG and anandamide and was unaffected by inhibitors of the synthesis of 2AG. In contrast, inhibiting phospholipid synthesis blocked this potentiation, consistent with LPI being an endogenous GPR55 agonist. Moreover, phospholipid synthesis blockade in the presynaptic cell blocked the burst-evoked CBD-sensitive axonal Ca^{2+} elevation. Although this result suggests an autoreceptor mode for GPR55 during repetitive spiking, further studies are needed to establish the exact source of the GPR55 ligand(s). It is also an open question whether GPR55 acts at other synaptic circuits. Finally, the finding that physiologically relevant GPR55 activation can be suppressed by CBD, a major constituent of *C. sativa*, has potential implications for psychiatry. CBD has a number of effects on humans, including antipsychotic and antiepileptic (25). Our results suggest a GPR55-dependent mechanism that may be involved in such effects. The facilitatory effect of GPR55 contrasts the action of CB_1 receptors that, if anything, inhibit neurotransmitter release (1, 2). $\Delta^9\text{THC}$, a major cannabis ingredient and a CB_1 receptor agonist, has variable effects on behavior depending on its dose (25, 26), whereas use of cannabis with high $\Delta^9\text{THC}$ and no CBD ("skunk") appears to increase risk of psychosis and memory impairment (27, 28). The present findings might help to understand the complex neurobiological basis of such effects.

Methods

A brief description: The full details are given in *SI Methods*.

Preparation. Transverse 350- μm hippocampal slices were obtained from 3- to 4-wk-old rats, 5- to 6-wk-old wild-type mice (CB57BL), age-matched GPR55 KO

mice (Gpr55^{tm1Lex}, involves 129/SvEvBrd \times C57BL/6J) and CB_1 KO mice (ABH background; kindly supplied by David Baker (Queen Mary University of London, London) and Catherine Ledent, (Institut de Recherche Interdisciplinaire en Biologie Humaine et Moléculaire, Brussels). Slices were transferred to the submersion recording chamber and superfused at 34 °C with oxygenated ACSF. Recordings in hippocampal cultures were performed at 20- to 24-d in vitro at 34 °C, adapting described routine (29); electrophysiological and pharmacological protocols were optimized for the corresponding tasks (*SI Methods*).

Imaging. Presynaptic CA3 or postsynaptic CA1 pyramidal cells were loaded in whole-cell mode with Alexa 594 and a Ca^{2+} indicator (Fluo-4, Fluo-8, or OGB-1) and examined by using a Radiance 2100 (Zeiss-Bio-Rad) based system as described (17, 30). Evoked Ca^{2+} responses were routinely documented as $\Delta G/R$ (18), where $\Delta G = G - G_0$ (the green channel signal G minus baseline fluorescence G_0), and R stands for the Alexa channel fluorescence.

Immunohistochemistry. We adapted the technique described (31): Slices were repeatedly washed in PBS and incubated first with the primary anti-GPR55 antibody (supplied by Ken Mackie) then with Alexa 488 conjugated Goat anti-rabbit secondary antibody; in colocalization experiments also with primary anti-VGLUT1 antibody and Goat anti-Guinea Pig Alexa 568 secondary antibody (*SI Methods*). Fluorescent puncta labeling was quantified by using a blind threshold sliding ImageJ algorithm (Gabriel Lapointe, University of Montreal, Montreal), and label colocalization was analyzed with an unsupervised ImageJ colocalization algorithm (Pierre Bourdoncle, Université Paris Descartes, Paris). T1117 was applied in live slices near CA3 pyramids through a pressurized pipette under constant monitoring (*SI Methods*).

ACKNOWLEDGMENTS. We thank Ken Mackie, Dimitri Kullmann, Peter Greasley, Andrew Irving, Leslie Iversen, and Raphael Mechoulam for invaluable comments; David Baker and Catherine Ledent for supplying CB_1 KO mice; and Ken Mackie for supplying GPR55 antibodies. This work was supported by the Wellcome Trust, the Medical Research Council, the Biotechnology and Biological Sciences Research Council, a European Research Council Advanced Grant (to D.A.R.), and National Institutes of Health Grants DA-3672 and DA-09789 (to R.A.R.).

- Wilson RI, Nicoll RA (2002) Endocannabinoid signaling in the brain. *Science* 296(5568):678–682.
- Katona I, Freund TF (2008) Endocannabinoid signaling as a synaptic circuit breaker in neurological disease. *Nat Med* 14(9):923–930.
- Sawzdargo M, et al. (1999) Identification and cloning of three novel human G protein-coupled receptor genes GPR52, PsiGPR53 and GPR55: GPR55 is extensively expressed in human brain. *Brain Res Mol Brain Res* 64(2):193–198.
- Ryberg E, et al. (2007) The orphan receptor GPR55 is a novel cannabinoid receptor. *Br J Pharmacol* 152(7):1092–1101.
- Henstridge CM, et al. (2011) Minireview: Recent developments in the physiology and pathology of the lysophosphatidylinositol-sensitive receptor GPR55. *Mol Endocrinol* 25(11):1835–1848.
- Johns DG, et al. (2007) The novel endocannabinoid receptor GPR55 is activated by atypical cannabinoids but does not mediate their vasodilator effects. *Br J Pharmacol* 152(5):825–831.
- Oka S, Nakajima K, Yamashita A, Kishimoto S, Sugiura T (2007) Identification of GPR55 as a lysophosphatidylinositol receptor. *Biochem Biophys Res Commun* 362(4):928–934.
- Henstridge CM, et al. (2009) The GPR55 ligand L-alpha-lysophosphatidylinositol promotes RhoA-dependent Ca^{2+} signaling and NFAT activation. *FASEB J* 23(1):183–193.
- Ross RA (2009) The enigmatic pharmacology of GPR55. *Trends Pharmacol Sci* 30(3):156–163.
- Lauckner JE, et al. (2008) GPR55 is a cannabinoid receptor that increases intracellular calcium and inhibits M current. *Proc Natl Acad Sci USA* 105(7):2699–2704.
- Waldeck-Weiermair M, et al. (2008) Integrin clustering enables anandamide-induced Ca^{2+} signaling in endothelial cells via GPR55 by protection against CB_1 -receptor-triggered repression. *J Cell Sci* 121(Pt 10):1704–1717.
- Ryan D, Drysdale AJ, Lafourcade C, Pertwee RG, Platt B (2009) Cannabidiol targets mitochondria to regulate intracellular Ca^{2+} levels. *J Neurosci* 29(7):2053–2063.
- Emptage NJ, Reid CA, Fine A (2001) Calcium stores in hippocampal synaptic boutons mediate short-term plasticity, store-operated Ca^{2+} entry, and spontaneous transmitter release. *Neuron* 29(1):197–208.
- Lauri SE, et al. (2003) A role for Ca^{2+} stores in kainate receptor-dependent synaptic facilitation and LTP at mossy fiber synapses in the hippocampus. *Neuron* 39(2):327–341.
- Henneberger C, Papouin T, Oliet SH, Rusakov DA (2010) Long-term potentiation depends on release of D-serine from astrocytes. *Nature* 463(7278):232–236.
- Hanse E, Gustafsson B (2001) Paired-pulse plasticity at the single release site level: An experimental and computational study. *J Neurosci* 21(21):8362–8369.
- Scott R, Lalic T, Kullmann DM, Capogna M, Rusakov DA (2008) Target-cell specificity of kainate autoreceptor and Ca^{2+} -store-dependent short-term plasticity at hippocampal mossy fiber synapses. *J Neurosci* 28(49):13139–13149.
- Oertner TG, Sabatini BL, Nimchinsky EA, Svoboda K (2002) Facilitation at single synapses probed with optical quantal analysis. *Nat Neurosci* 5(7):657–664.
- Emptage NJ, Reid CA, Fine A, Bliss TV (2003) Optical quantal analysis reveals a presynaptic component of LTP at hippocampal Schaffer-associational synapses. *Neuron* 38(5):797–804.
- Kobe F, et al. (2012) 5-HT7R/G12 signaling regulates neuronal morphology and function in an age-dependent manner. *J Neurosci* 32(9):2915–2930.
- Rusakov DA, Fine A (2003) Extracellular Ca^{2+} depletion contributes to fast activity-dependent modulation of synaptic transmission in the brain. *Neuron* 37(2):287–297.
- Daly CJ, et al. (2010) Fluorescent ligand binding reveals heterogeneous distribution of adrenoceptors and 'cannabinoid-like' receptors in small arteries. *Br J Pharmacol* 159(4):787–796.
- Wu LG, Saggau P (1994) Presynaptic calcium is increased during normal synaptic transmission and paired-pulse facilitation, but not in long-term potentiation in area CA1 of hippocampus. *J Neurosci* 14(2):645–654.
- Dityatev A, Rusakov DA (2011) Molecular signals of plasticity at the tetrapartite synapse. *Curr Opin Neurobiol* 21(2):353–359.
- Russo E, Guy GW (2006) A tale of two cannabinoids: The therapeutic rationale for combining tetrahydrocannabinol and cannabidiol. *Med Hypotheses* 66(2):234–246.
- Bhattacharyya S, et al. (2010) Opposite effects of delta-9-tetrahydrocannabinol and cannabidiol on human brain function and psychopathology. *Neuropsychopharmacology* 35(3):764–774.
- Morgan CJ, Schafer G, Freeman TP, Curran HV (2010) Impact of cannabidiol on the acute memory and psychotomimetic effects of smoked cannabis: Naturalistic study: Naturalistic study [corrected]. *Br J Psychiatry* 197(4):285–290.
- Di Forti M, et al. (2009) High-potency cannabis and the risk of psychosis. *Br J Psychiatry* 195(6):488–491.
- Ermolyuk YS, et al. (2012) Independent regulation of Basal neurotransmitter release efficacy by variable Ca^{2+} influx and bouton size at small central synapses. *PLoS Biol* 10(9):e1001396.
- Scott R, Rusakov DA (2006) Main determinants of presynaptic Ca^{2+} dynamics at individual mossy fiber-CA3 pyramidal cell synapses. *J Neurosci* 26(26):7071–7081.
- Jensen JB, Lauckner JE (2006) Novel probes for G-protein-coupled receptor signaling. *J Neurosci* 26(42):10621–10622, discussion 10622.